Meteorol Atmos Phys
DOI 10.1007/s00703-012-0214-8

ORIGINAL PAPER

Tracing the origins and propagation of pre-tropical storm Debby (2006) mesoscale convective systems using pattern recognition and image fusion

Chaunté W. Lacewell · Abdollah Homaifar · Yuh-Lang Lin

Received: 20 January 2012 / Accepted: 24 September 2012

Abstract This study is focused on developing pattern recognition and image fusion techniques to trace the origins and propagation of the pre-tropical storm (pre-TS) Debby (2006) mesoscale convective systems (MCSs) and African easterly waves (AEWs) using satellite imagery. These MCSs could be generating over mountains in North Africa and going through complicated splitting and merging processes. Therefore, an objectively analyzed MCS movement is essential. This study presents a technique which traces extracted features to find the origin of TS Debby. This technique produces a fused image with the most relevant information from water vapor and infrared satellite images, segments the cloud top height satellite images by clustering clouds, and tracks clouds to determine the origin of TS Debby (2006). The presented technique could be applied to other AEWs and MCSs which lead to tropical cyclogenesis to improve the numerical weather prediction over data sparse areas, such as over eastern and central North Africa.

1 Introduction

A tropical cyclone (TC) is a non-frontal synoptic-scale warm core low-pressure system that originates over tropical or subtropical oceans and contains organized deep convection and a defined cyclonic surface wind circulation (Lin 2007). The formation of TCs over the eastern Atlantic Ocean region, off the North African coast, remains an important research topic, which is poorly understood due to the lack of an adequate scientific understanding of the physical mechanisms involved and sparsity of data in the area. TCs contain groups of thunderstorms which are often organized in mesoscale convective systems (MCSs) (Lin 2007). Prior studies have shown that the source disturbances for the development of Atlantic TCs are African easterly waves (AEWs) with MCSs embedded in them (Berry and Thorncroft 2005; Reed et al. 1977). The AEWs are prominent in the Northern Hemisphere from June until early October and usually have a wavelength of 2,000–4,000 km, a phase speed of 7–9 m s^{-1}, and a period of approximately 3–5 days (Reed et al. 1977; Zawislak and Zipser 2010). Although only a few AEWs organize and develop into a TC, the AEW-induced TCs account for about 60 % of the Atlantic Ocean's TCs and for about 85 % of major hurricanes (Landsea 1993; Lin et al. 2012; Pielke and Landsea 1998). Classification and prediction of TCs are known to be a difficult task due to the lack of understanding of physical mechanisms that are involved in the cyclogenesis, the technical term for the development and strengthening stage of a TC.

Forecasters have difficulty representing these storms accurately in numerical weather prediction (NWP) models as well as in detecting and predicting the early stages of cyclogenesis with confidence (Piñeros and Ritchie 2006). Therefore, the physical processes associated with TC development are a research topic of great interest. This research topic is of importance to forecasters, because it helps them locate signs of cyclogenesis and the origin of many TCs. Having this information will help the public prepare for TCs in a timely manner. Earlier studies, with

Responsible Editor: J.-F. Miao.

C. W. Lacewell · A. Homaifar (✉)
Department of Electrical and Computer Engineering, North Carolina A&T State University, Greensboro, NC 27411, USA
e-mail: Homaifar@ncat.edu

Y.-L. Lin
Department of Physics, North Carolina A&T State University, Greensboro, NC 27411, USA

Published online: 27 November 2012

the assistance of satellite observations, have observed that MCSs which are embedded within AEWs can lead to TC development (Simpson et al. 1968). Analysis of satellite observations is an effective approach for understanding atmospheric properties and is widely used for weather forecasting and prediction purposes (Mandal et al. 2005). One method to reliably detect or predict the development of a TC is to examine the evolution of cloud clusters using satellite observations. However, determining whether cloud clusters will merge into an AEW–MCS and then develop into a TC has been shown by many to be a difficult task (Piñeros et al. 2010).

Objectively analyzed AEW–MCS movement using satellite observations is essential to understand the formation and propagation of developing TCs. Grazzini et al. (2001) stated that pixel's gray level values from satellite observations give impressive insights on cloud structures in a precise way. This fact is the basis of ongoing research to help forecasters predict or analyze TC evolution, formation, and intensity. This research focused on expanding the research on determining the origins of pre-TC AEW and MCSs using solely satellite observations. Forecasters will be able to use the proposed techniques to assist in their determinations of the origins of these TCs which, in turn, will assist them in the difficult task of predicting the storms. The main focus of this research was to develop image fusion and pattern recognition techniques to trace the origins and propagation of the pre-tropical storm (TS) Debby (2006) MCSs using satellite imagery.

Image fusion is the process of combining images from multiple sources, such as sensors, in order to make inferences about an event of interest, such as weather. This process was used to combine images from different instrument channels in an efficient manner in order to obtain the most important characteristics from each source. Pattern recognition is the process of assigning a label to a given instance. Pattern recognition techniques for this research were used to separate (or group) the data into different clusters (or classes). Due to the lack of understanding of AEW–MCS formation and propagation, the groups were based on some inherent similarity measure using unsupervised techniques. Forecasters can use the image fusion and pattern recognition techniques to improve the accuracy of numerical simulations of the development and strengthening stages of a TC. This improvement was gained by allowing a reasonable model initialization scheme once the calculated origin was included in the model domain. As hypothesized by Hodges and Thorncroft (1997) and Lin et al. (2012), the mountains in East Africa and Arabian Peninsula may play a role in initiating the AEW and its associated MCSs along with other environmental factors. These factors were analyzed and their hypothesis was validated.

2 Mesoscale convective systems and African easterly waves

2.1 Mesoscale convective systems

MCSs are considered to be an organized cluster of thunderstorms with a spatial scale of 100–1,000 km which is approximately 1–10° in latitude (Lin 2007). MCSs are usually circular or linear in shape. However, smaller convective systems can sometimes merge into a larger, elliptical MCS; the underlying convective cells can be hidden by the extensive cloud shield. MCSs can form in different environmental conditions. Some form in a moist environment with strong wind shear and others occur in a moist environment with no wind shear. These MCSs can sometimes merge together and, under the right conditions, they form TCs.

In infrared satellite images, a MCS looks like a well-organized mesoscale cloud cluster, which has a circular or oval shape depending on upper level wind strength. In this research, the clouds of interest were high- and middle-level clouds due to the fact that higher clouds usually have longer life cycles. With that in mind, this research separated the middle- and high-level clouds into classes. When separating middle-level clouds, the classes included altocumulus, altostratus, and nimbostratus clouds. Cirrus, cirrostratus, anvil cirrus, and cirrocumulus are types of clouds that were included when separating high-level clouds. The preceding cloud types were important in this research, especially when tracking the MCSs to find the origin of a tropical cyclone.

2.2 African easterly waves

Tracking the AEW and MCS systems to their origins is essential in helping understand the interactions involved in the formation of AEWs and MCSs over North Africa. As mentioned earlier, tropical cyclogenesis is often led by disturbances in the atmosphere such as propagating AEWs. The AEWs are the dominant synoptic-scale atmospheric wave systems in West Africa and are the main precursors of TCs in the Atlantic Ocean. Satellite data were used in the work presented by Simpson et al. (1968) and Carlson (1969) which traced the Atlantic tropical cyclogenesis from disturbances over West and Central Africa around 10°N, but not in East Africa. Note that in these studies, tracking the MCSs in satellite images is an alternative way of tracking AEWs. AEWs likely develop from instabilities in the mid-tropospheric African easterly jet (AEJ) and can develop sustained convection; in some cases, these AEWs will further develop into a TC (e.g., Burpee 1972). Inconsistency in AEW activity modulates TC activity; therefore, understanding the circumstances under which

AEWs dissipate has the potential to enhance predictability of tropical cyclogenesis and TC formation (Agudelo et al. 2011).

Hill and Lin (2003) and Lin et al. (2005) suggested that the Ethiopian Highlands region is a favorable location for the development of AEWs which are formed over land, within the tropical rain forest belt of equatorial Africa, or develop downstream of mountain ranges. This disturbance then propagates to the western coastline of Africa where some MCSs develop into TCs. This occurs when the MCSs form at the crest of a wave-like structure and exhibit banding features (Laing and Fritsch 1993). Hodges and Thorncroft (1997) concluded in their study that majority of MCSs originate near the EH and Hill and Lin (2003) observed that the MCSs that form on the lee side of the EH propagate downstream of the EH region with the associated AEW. Mozer and Zehnder (1996) found through simulation that the low-level easterly flow over the Atlas and Hoggar Mountains in Western Africa results in a barotropically unstable jet which produces many lee vortices that propagate downstream from the mountain. This region is also where the AEJ occurs as a result of the strong temperature gradient over the surface of North Africa in response to the differences in climate between the Sahara and the African rain belt. Pytharoulis and Thorncroft (1995) suggested that the locations of the AEWs are closely associated with the movement of the AEJ. Grist (2002) found that AEJs behave differently in wet and dry years. Because AEWs are closely associated, AEWs differ as well. AEWs are often associated with MCSs while they travel westward (Lin et al. 2012; Laing and Fritsch 1993) which helps make AEWs detectable from satellite imagery.

3 Methodology

The purpose of this paper is to present the results of research which used image fusion and pattern recognition techniques to trace the origins and propagations of pre-TS Debby's (2006) mesoscale convective systems. The block diagram for the methodology used is displayed in Fig. 1 and the steps below have been performed for this study.

The programs used for visualization and computations in this research are MathWorks Incorporated's Matlab, ITT Visual Information Solutions' IDL, and National Oceanic and Atmospheric Administration's (NOAA's) Weather and Climate Toolkit. Matlab is a well-known high-level language that performs computationally exhaustive tasks faster, therefore it was used to perform the main tasks of image fusion, clustering, feature extraction and tracking. IDL and NOAA's Weather and Climate Toolkit were solely used in this study to produce the satellite images needed.

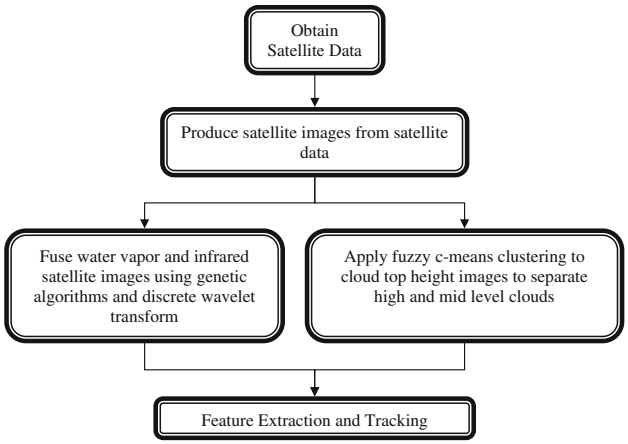

Fig. 1 Block diagram for the methodology used to trace the origins and propagation of pre-tropical storm Debby (2006)

3.1 Image fusion

Image fusion is a process of combining images from multiple sources to estimate or predict an event of interest like weather (Hall and McMullen 2004). The accuracy of the initialization scheme in numerical simulations of TC AEWs and MCSs was improved by fusing images. The accuracy was improved by providing more detailed information than individual VIS, IR, and WV data can give alone. When fusing images, it is important that the source images used for fusion are similar in some way. For this study, the source satellite images had gray level values and were scaled in the same manner in order to make sure that the fusion process was accurate.

Prior research in weather forecasting has verified that it is quite difficult to obtain all necessary information from a single satellite image. Because of this, it is beneficial to fuse images from multiple sensors into a single image which contains the most relevant information from source images (Mumtaz et al. 2008). A main disadvantage of current image fusion techniques is that most techniques simply merge the image data together which results in information loss and a change in spectral characteristics of an image (Wehrmann et al. 2004). Research has been done on different image fusion techniques which produce an accurately fused image that displays the most significant characteristics of the source.

Lacewell et al. (2010) proposed an image fusion method that uses discrete wavelet transform (DWT) and an optimization tool. Figure 2 displays the block diagram for this method. DWT is used in this technique to decompose the images into a multi-resolution representation that capture coarse and detailed information. This representation was used in the optimization tool (e.g., Genetic Algorithm) to determine the optimal weights of the water vapor (WV) and infrared (IR) satellite images

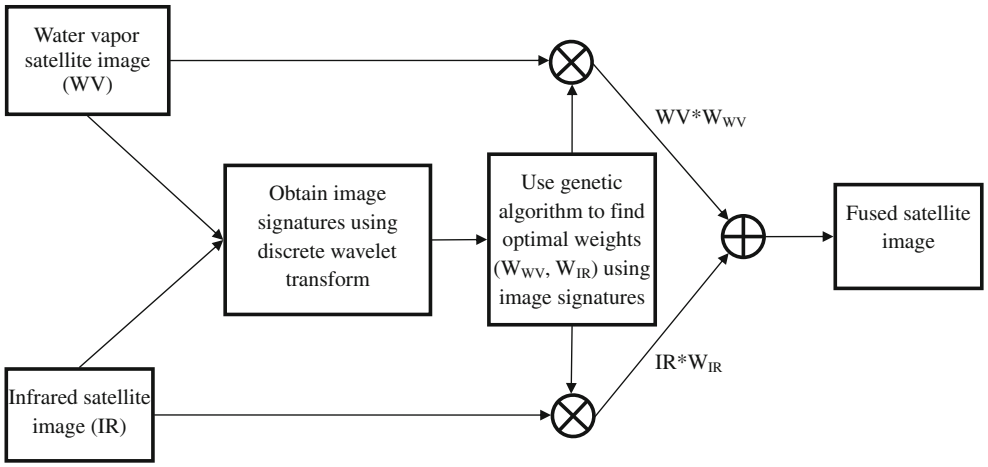

Fig. 2 Block diagram of image fusion technique

for the produced fused image. Using the DWT representation is computationally inexpensive when compared to processing the entire image.

3.2 Clustering

Clustering refers to the process of assigning a label to members of a population where members with similar measurable characteristics are placed in the same class. Clustering can be divided into supervised and unsupervised clustering; but for this research, unsupervised clustering was used. Supervised clustering is the process of clustering where there is prior knowledge of the classes in which the data belong. Unsupervised clustering refers to the clustering process where nothing is known concerning the membership of the data to specific classes (Theodoridis and Koutroumbas 2003). This method is useful in processing satellite imagery due to the fact that pattern information in the satellite images is usually unknown.

Clustering was implemented in Matlab to segment the images which were produced with Meteosat second generation's (MSG's) cloud top height (CTH) dataset. To simplify the CTH imagery, the high- and middle-level clouds were extracted using morphological operators. These operators included *bwareaopen* which removes all objects containing less than a specified number of pixels and *imfill* which fills in any holes in the image. Once the image contained the relevant clouds, it was then converted to the French *Commission Internationale de l'éclairage* (CIE) L*a*b* color space to simplify the clustering stage. The clustering technique that was used in this research was the fuzzy C-means (FCM) algorithm which is a method of partitioning a collection of N vectors into c clusters G_i (where $i = 1, 2, \ldots, c$) that allowed a data point to belong to two or more clusters. For this study, the image was partitioned into three clusters which represented the high-level clouds, middle-level clouds, and all other pixels. The general goal of FCM was to find the cluster centers which minimize how dissimilar data elements are. This dissimilarity can be measured using a dissimilarity function. The steps for FCM clustering algorithm are as follows (Albayrak and Amasyali 2003):

1. Randomly initialize the binary membership matrix $U = [u_{ij}]$ using $\sum_{i=1}^{c} u_{ij} = 1, \forall j = 1, \ldots, n$ where $u_{ij} \in [0, 1]$, and c and n are the number of clusters and inputs, respectively.
2. At k-step, calculate the cluster centers c_i.

$$c_i = \frac{\sum_{j=1}^{n} u_{ij}^m x_j}{\sum_{j=1}^{n} u_{ij}^m}$$

where $m \in [1, \infty]$ is a weighting exponent and x_j is the data points.

3. Compute dissimilarity function J between centroids and data points

$$J(U, c_1, c_2, \ldots, c_c) = \sum_{i=1}^{c} \sum_{j=1}^{n} u_{ij}^m d_{ij}^2$$

c_i is the center of cluster i, and d_{ij} is the Euclidean distance between the ith cluster center and jth data point.

4. Compute new u_{ij}. If $\|U(k+1) - U(k)\| < \varepsilon$, the user-defined sensitivity threshold, then stop. Otherwise go to step 2.

$$u_{ij} = \frac{1}{\sum_{k=1}^{c} \left(\frac{d_{ij}}{d_{kj}}\right)^{\frac{2}{m-1}}}$$

By iteratively updating the cluster centers and the membership grades for each data point, FCM iteratively moves the cluster centers to the "correct" location within a data set (Albayrak and Amasyali 2003). This technique

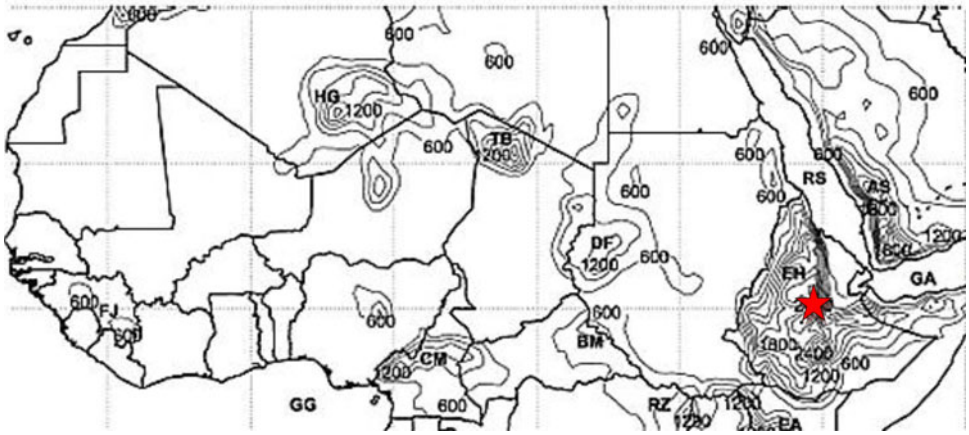

Fig. 3 Terrain data for Northern Africa with labels to indicate major geographical features. Asir Mountains (AR), Bongo Massif (BM), Cameroon Highlands (CM), Darfur Mountains (DF), Eastern Arc Mountains (EA), Ethiopian highlands (EH), Futa Jallon Highlands (FJ), Gulf of Aden (GA), Gulf of Guinea (GG), Hoggar Mountains (HG), Ruwenzori Mountains (RZ), and Tibesti Mountains (TB) (Lin et al. 2005). The *red star* indicates the peak of EH (color figure online)

assists in distinguishing between the middle- and high-level clouds in the CTH imagery.

3.3 Feature extraction and tracking

In image processing, feature extraction is the technique for acquiring relevant features that help to better understand the data. There are many feature extraction methods, but there are only a few that are commonly used. Object tracking is an image processing problem that can benefit from an accurate feature extraction method, for example, tracing the origins and propagations of pre-TCs. The feature extraction and tracking portion of this research was the most important part in tracing the origin and propagations of pre-TS Debby (2006). For this procedure, the scale and orientation adaptive mean shift tracking (SOAMST) method, which was proposed by the work given by Ning et al. (2010), was used. This algorithm can solve problems of estimating the scale and orientation changes of a target and it is based on the area of the target and the corrected second order central moments. A key to successful results is to select the region (or object) that is being tracked and set the parameters to an appropriate value. The satellite images used in this research were taken in 3-h intervals. Therefore, this algorithm must have an appropriate value for the search size so it can accommodate this interval. When implementing this algorithm, an appropriate search size to locate the target object was set to 10; this size was determined through trial and error by comparing the center of a cloud with a known location. This parameter may vary depending on the application of the algorithm, but for this application, this search size increased the accuracy of the tracking procedure to accommodate the cloud movement in the 3-h interval. The implementation of this algorithm is summarized below:

1. Initialize the position, y_0, of the target candidate model and then calculate the target model using

$$\hat{q} = \frac{\sum_{i=1}^{n} k\left(\left\|x_i^*\right\|^2\right)\delta\left[b\left(x_i^*\right) - f\right]}{\sum_{i=1}^{n} k\left(\left\|x_i^*\right\|^2\right)}$$

where δ is the Kronecker delta function, $b(x_i*)$ associates the pixel x_i* to the histogram bin, f is the feature in the target model, and $k(x)$ is an isotropic kernel profile.

2. Initialize the iteration number $k \leftarrow 0$.

3. Calculate the target candidate model $\hat{p}(y_0)$ in the current image frame using

$$\hat{p}(y_0) = \frac{\sum_{i=1}^{n_h} k\left(\left\|\frac{y_0 - x_i}{h}\right\|^2\right)\delta[b(x_i) - f]}{\sum_{i=1}^{n_h} k\left(\left\|\frac{y_0 - x_i}{h}\right\|^2\right)}$$

where x_i are pixels in the target candidate region centered at y_0 where $i = 1,\ldots, n$, and h is the bandwidth.

4. Calculate the weight vector $\{w_i\}_{i=1,2,\ldots,n}$ using

$$w_i = \sum_{u=1}^{m} \sqrt{\frac{\hat{q}_u}{\hat{p}_u(y_0)}}\delta[b(x_i) - f]$$

where δ and $b(x_i)$ have the same meaning as in step 1.

5. Calculate the new position y_1 of the target candidate model using

$$y_1 = \frac{\sum_{i=1}^{n_h} x_i w_i}{\sum_{i=1}^{n_h} w_i}.$$

6. Let $\|y_1 - y_0\| \rightarrow d$. Set the error threshold, ε (default is 0.1), and the maximum iteration number, N (default is 15).

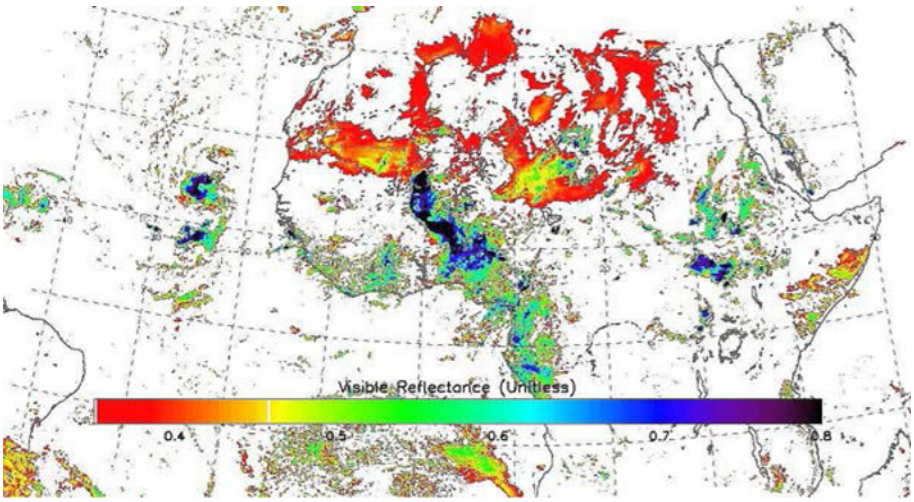

(a)

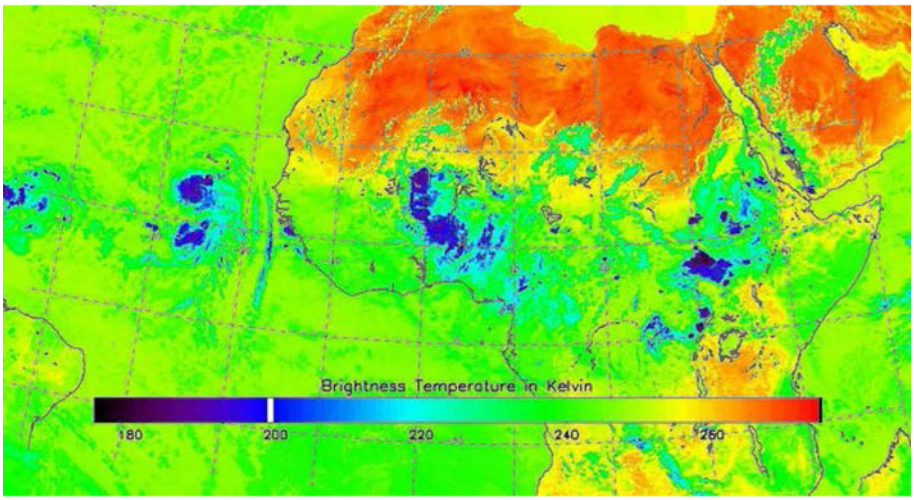

(b)

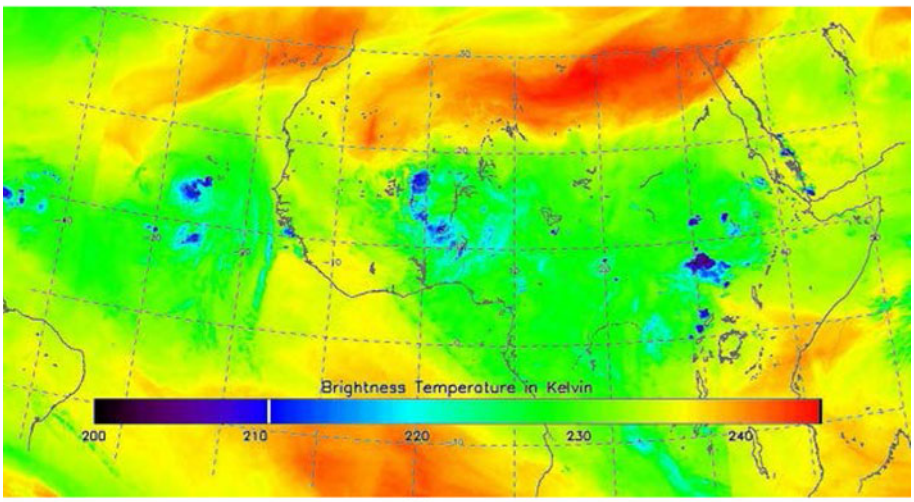

(c)

Fig. 4 Examples of the satellite images generated from the GridSat data for **a** visual channel, **b** infrared channel, and **c** infrared water vapor channel for 8/22/12Z

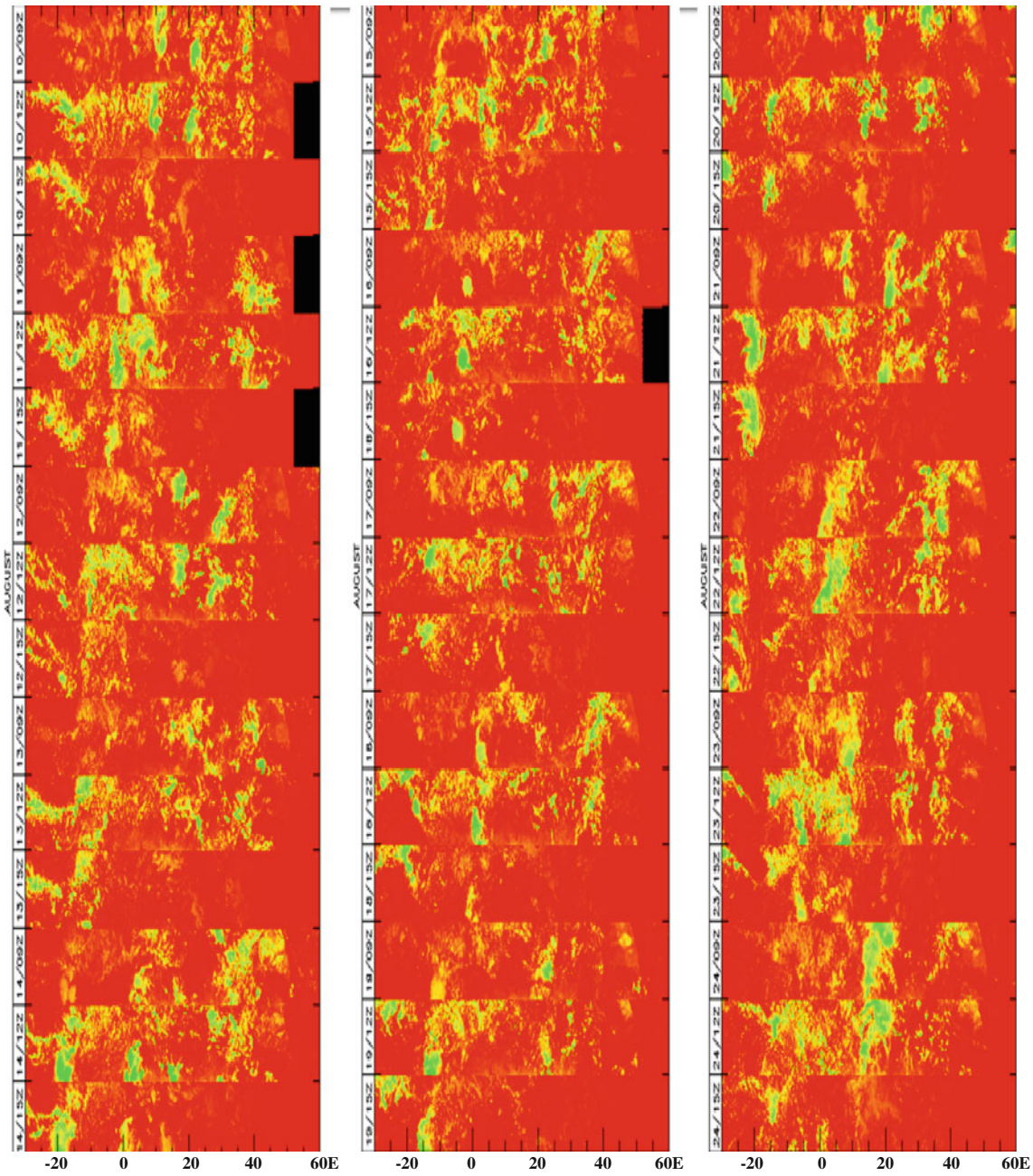

Fig. 5 Hovmöller diagram of the GridSat visual channel from 8/10/09Z to 8/24/12Z in 3-h intervals for the pre-Debby (2006) system. The visual channel is only visible during daylight, therefore only 9–15Z for each day are shown

If $(d < \varepsilon$ or $k \geq N)$ Stop and go to step 7
Otherwise $k + 1 \rightarrow k$ and go to step 3

7. Estimate the width, height, and orientation from the target candidate model using

$$\text{Cov} = \begin{bmatrix} f_{11} & f_{12} \\ f_{21} & f_{22} \end{bmatrix} * \begin{bmatrix} a^2 & 0 \\ 0 & b^2 \end{bmatrix} * \begin{bmatrix} f_{11} & f_{12} \\ f_{21} & f_{22} \end{bmatrix}^T$$

where the vectors $(f_{11}, f_{21})^T$ and $(f_{12}, f_{22})^T$ represent the orientation of the two main axes of the target, A is the estimated area of the target, and λ_1 and λ_2 are the eigenvalues of the covariance matrix, while $a = \sqrt{\lambda_1 A/(\pi\lambda_2)}$, and $b = \sqrt{\lambda_2 A/(\pi\lambda_1)}$.

8. Estimate the initial target candidate model for the next frame using

$$(x - y_1) * \text{Cov}_2^{-1} * (x - y_1)^T \leq 1$$

At the conclusion of this algorithm, the origin of the TC is enclosed in an ellipse.

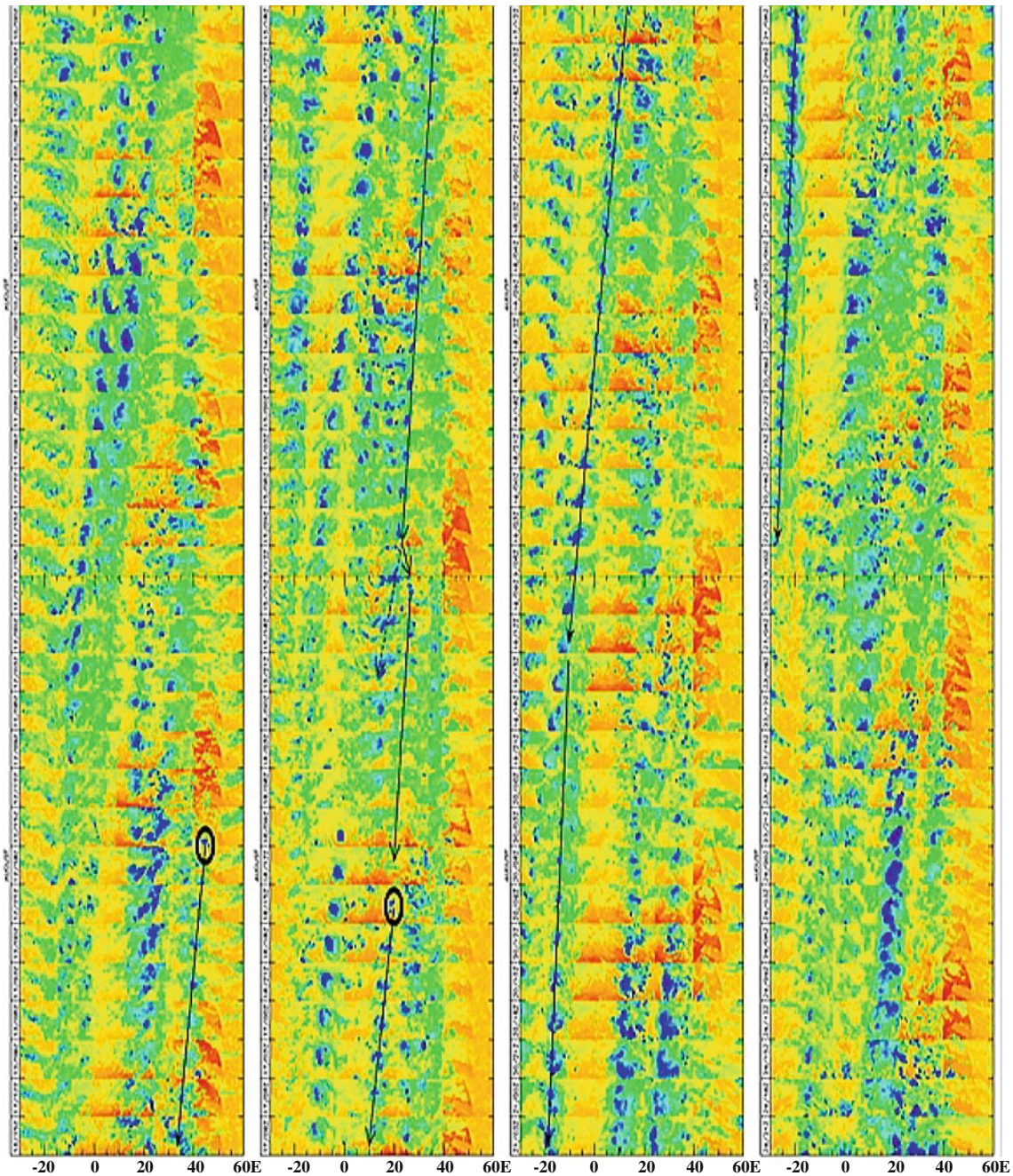

Fig. 6 Hovmöller diagram of the GridSat infrared channel from 8/10/00Z to 8/24/12Z in 3-h intervals for the pre-Debby (2006) system with manually estimated tracks superimposed. The *solid lines* represent the track of pre-Debby (2006), while the *dashed lines* indicate where a splitting process has occurred. These tracks are produced manually therefore they are estimates and are not fully accurate

4 Case description, analysis and discussion

4.1 Case description

The track of the pre-TS Debby (2006) disturbance was analyzed previously by Lin et al. (2012) using Meteosat-8 satellite imagery and the Advanced Research Weather Research and Forecasting (ARW) model. In their study, a cloud cluster prior to pre-TS Debby (2006) MCS could be traced back to the region of Ethiopian Highlands and Asir Mountains around 8/11/00Z. For convenience, Fig. 3 shows the locations of the following geographical features: Asir Mountains (AR), Bongo Massif (BM), Cameroon Highlands (CM), Darfur Mountains (DF), Eastern Arc Mountains (EA), Ethiopian highlands (EH), Futa Jallon Highlands (FJ), Gulf of Aden (GA), Gulf of Guinea (GG),

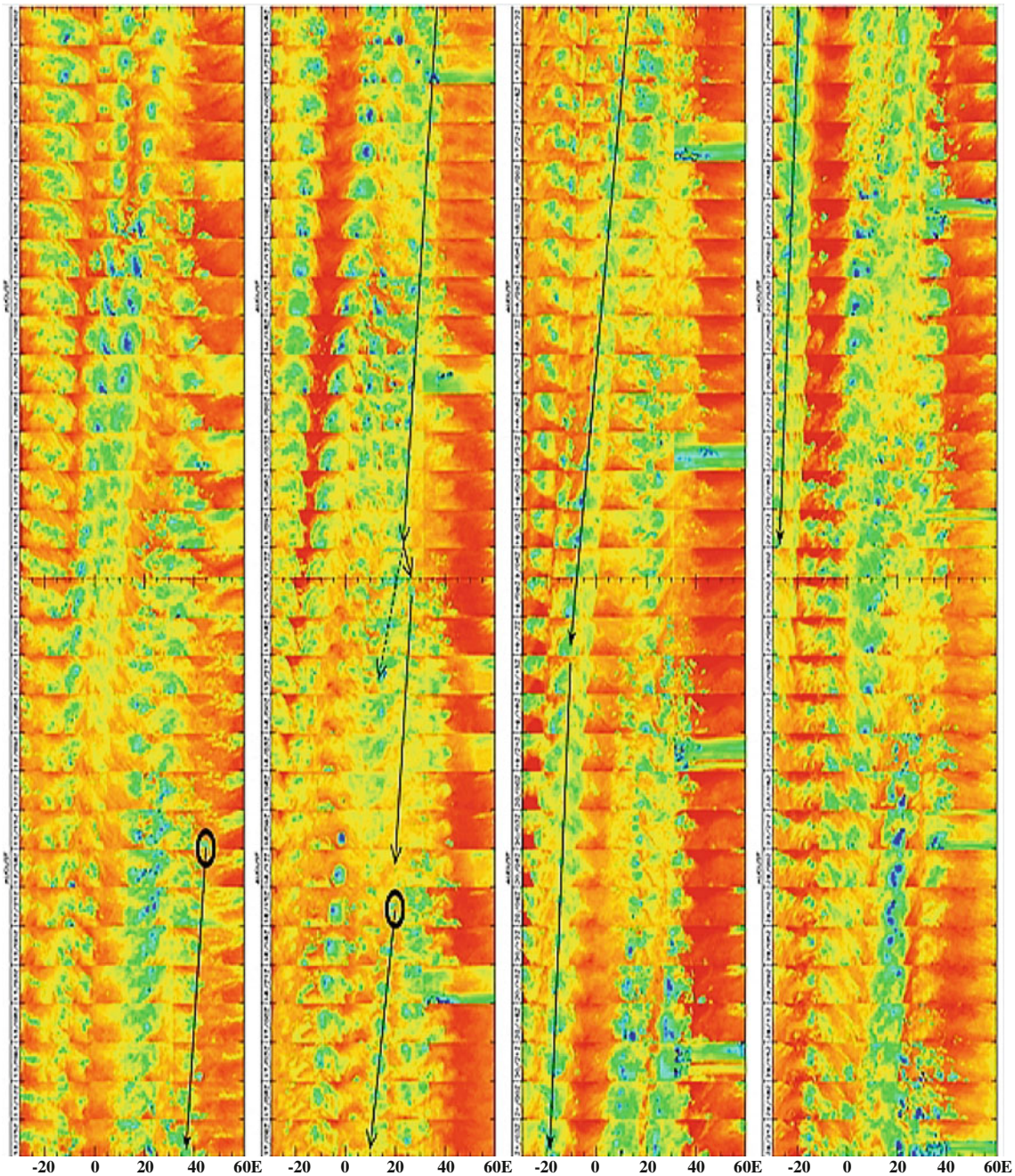

Fig. 7 Hovmöller diagram of the GridSat water vapor channel from 8/10/00Z to 8/24/12Z in 3-h intervals for the pre-Debby (2006) system with manually estimated tracks superimposed. The *solid lines* represent the track of pre-Debby (2006), while the *dashed lines* indicate where a splitting process has occurred. These tracks are produced manually therefore they are estimates and are not fully accurate. The moisture in the atmosphere is more visible when using this channel

Hoggar Mountains (HG), Ruwenzori Mountains (RZ), and Tibesti Mountains (TB).

4.2 Analysis

The pre-TS Debby (2006) MCSs were properly traced across Northern Africa to determine their origin and propagation. NOAA's GridSat data were used to produce satellite images using IDL. For a better understanding of GridSat's channels, Fig. 4 shows an example of the satellite images produced for the visual (VIS), IR, and WV channels, respectively. The VIS images display the visible reflectance, which is unitless, while the IR and WV channels display the brightness temperatures in Kelvin. These images were produced in black and white for fusion purposes.

Fig. 8 Hovmöller diagram of Meteosat second generation's cloud top height data from 8/10/00Z to 8/24/12Z in 3-h intervals for the pre-Debby (2006) system with manually estimated tracks superimposed. The *solid lines* represent the track of pre-Debby (2006). These tracks are produced manually therefore they are estimates and are not fully accurate but these tracks were easier to produce due to the height information

To manually estimate the track of the MCSs using this dataset, Hovmöller diagrams were produced in 3-h intervals. Figures 5, 6, and 7 display these Hovmöller diagrams for the region of interest (5°–15°N, 30°W–60°E) using the VIS, IR and WV channels, respectively. The VIS channel is only viewable during daylight hours; therefore, this Hovmöller diagram only contains the hours of 09Z–15Z for August 10–24. The IR and WV channels can be seen both day and night, making it easier to manually track the storm using these channels. Figures 6 and 7 show these diagrams with the estimated tracks superimposed. Many studies pertaining to satellite imagery are based on the IR channels because of its visibility throughout the day.

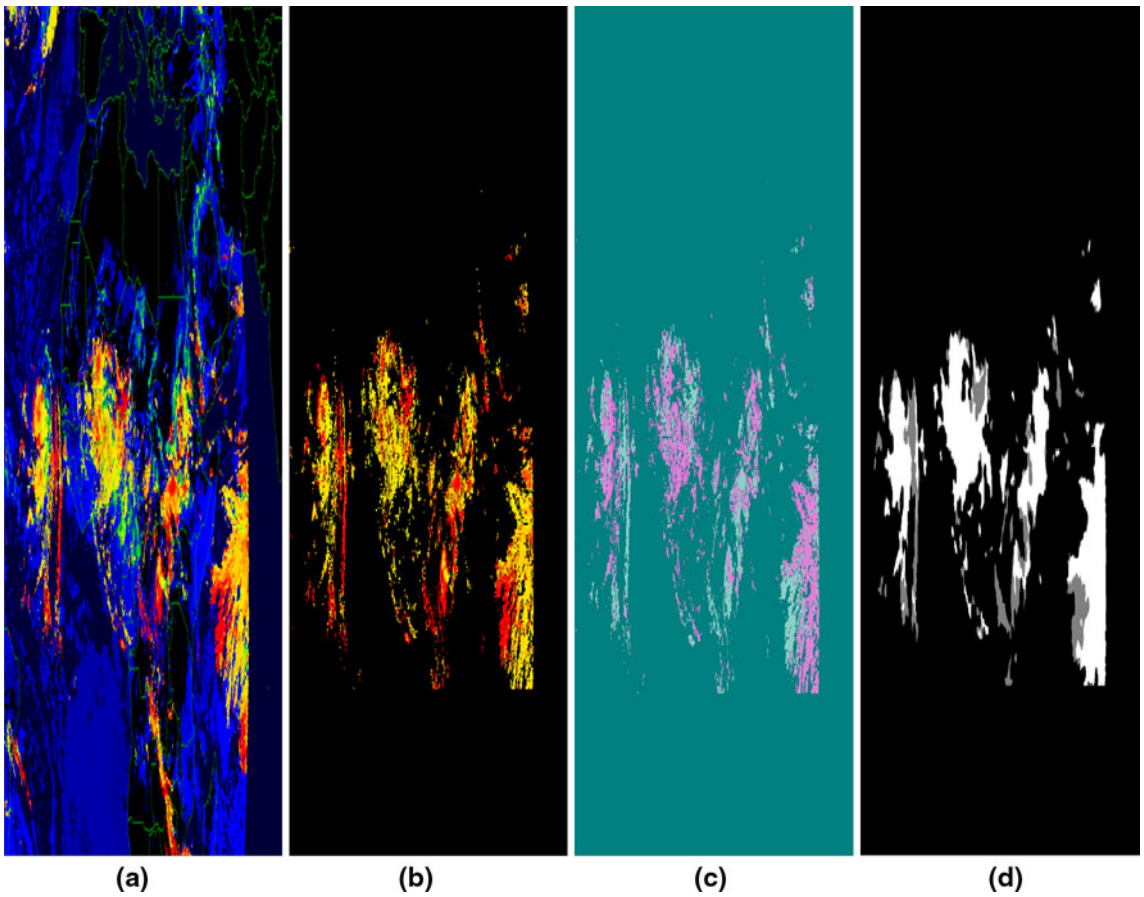

Fig. 9 These images illustrate the steps taken to cluster the cloud top height images into high- and middle-level clouds. **a** Cloud top height image for 8/22/12Z, **b** CTH image after image processing and morphological operators, **c** image changed to L*a*b* color space and **d** clustered image

Figure 8 shows the Hovmöller diagram of the CTH dataset with the estimated manual tracks superimposed. The MSG's CTH data were used for clustering as well as in the tracking stage of this work. This data were used because higher clouds have longer life cycles. Therefore, higher clouds have a better probability of living longer than lower clouds and clustering the CTH data simplifies the data by reducing the amount. Studies such as Jirak and Cotton (2007) suggest that more pronounced features are found in the lower troposphere which may be hidden by the cold cloud tops that are being analyzed in this study. This study was solely based on satellite imagery; therefore, the features in the clouds as well as the relationship between the middle-level and high-level clouds are of importance. Certain temperatures and features that are not visible in the high level clouds are visible in the middle-level clouds. If low-level clouds are of importance to a forecaster who uses this technique, the only modification that would need to be made is to change the number of clusters in the FCM algorithm from 3 to 4. This would identify the low-, middle-, and high-level clouds and all other pixels as clusters. The images in Fig. 9 illustrate the steps taken in the FCM algorithm to segment the CTH images into three classes.

Using Matlab, image fusion was applied to the IDL produced GridSat IR, and WV images. The image fusion technique proposed by Lacewell et al. (2010) was used to produce accurate fused images. The results were obtained using the optimization tool. The result of this image fusion method has minimal error and produces a fused image which contains the most important features from the source images. When the source images are of poor quality, this may cause error in the tracking stage because features could be undetected in the produced fused image. To reduce the possibility of error, IDL was used to produce high-quality satellite images directly from the satellite data which are essential to obtaining satisfactory results of the MCS tracks.

All image sequences were processed using the SOAMST algorithm since, unlike other tracking algorithms, it can adaptively calculate the scale and orientation of the object being tracked (Ning et al. 2010).

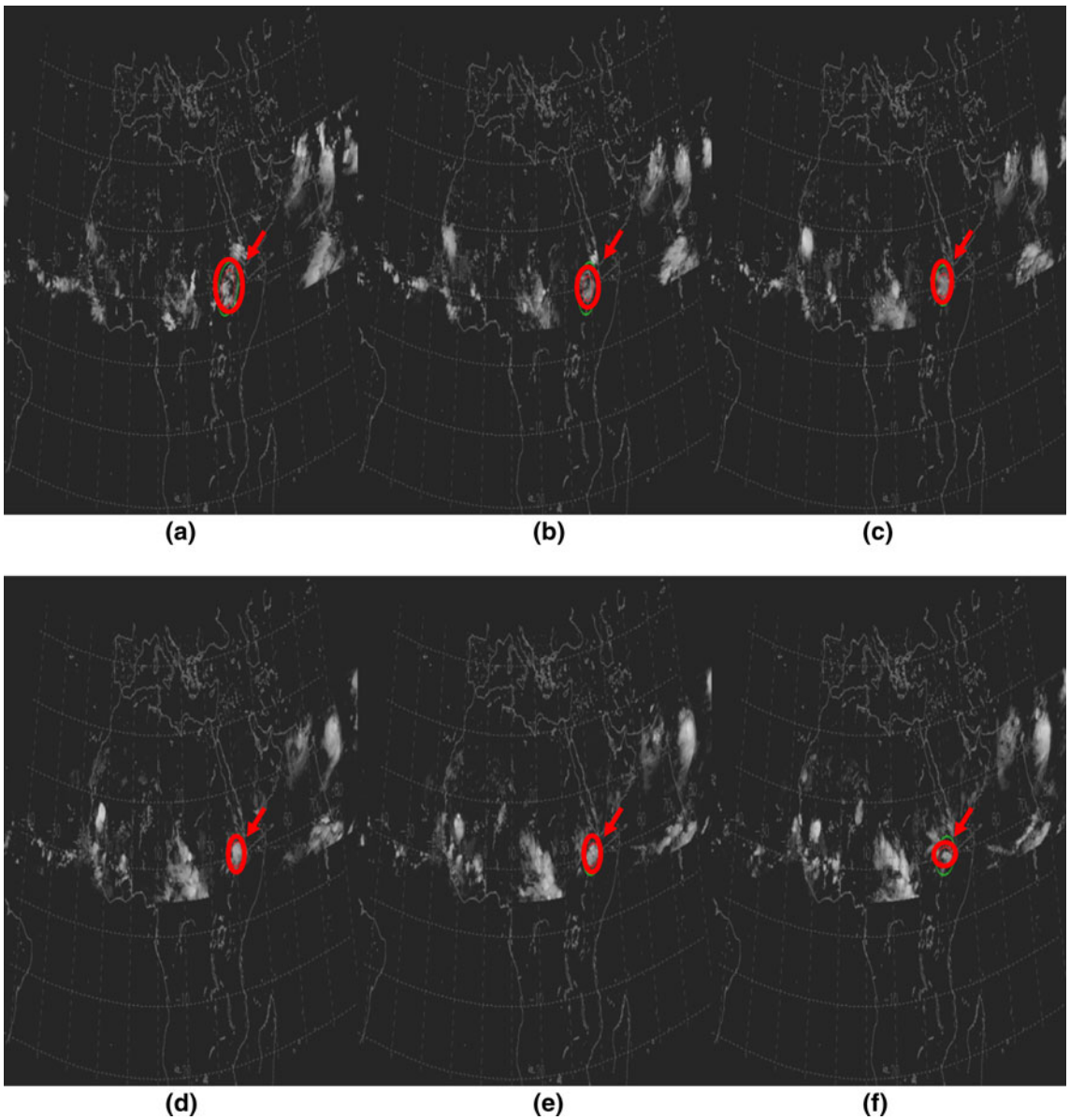

Fig. 10 Six frames produced by the SOAMST algorithm when applied to the GridSat infrared image sequence representing **a** 8/13/12Z, **b** 8/13/09Z, **c** 8/13/06Z, **d** 8/13/03Z, **e** 8/13/00Z, and **f** 8/12/21Z with *red arrow* and *circle* indicating tracked cloud (color figure online)

This algorithm was used to extract features using the second central moment (variance) and to track the MCSs for 8/10/00Z–8/24/21Z. Once selected, the algorithm then back tracks the storm to find the origin. In Figs. 10, 11, 12, and 13, six frames from the results of the SOAMST algorithm when applied to the IR, CTH, fused, and clustered image sequences, respectively, are shown. The tracked MCS is indicated by a circle and an arrow in each of these figures. In order to make the location of the MCS and cloud clusters more visible, the correct longitude and latitude grid lines were superimposed using IDL when needed.

4.3 Discussion

This research focused on developing image fusion and pattern recognition techniques to trace the origins and propagations of pre-TS Debby (2006) MCSs and AEWs using satellite imagery. There may be cases where MCSs do not occur during AEWs, but even in those cases, the technique presented in this study is still valid. The task was completed using image fusion technique proposed by Lacewell et al. (2010), clustering of clouds into three classes using the FCM algorithm, and feature extraction and tracking using the SOAMST algorithm which was

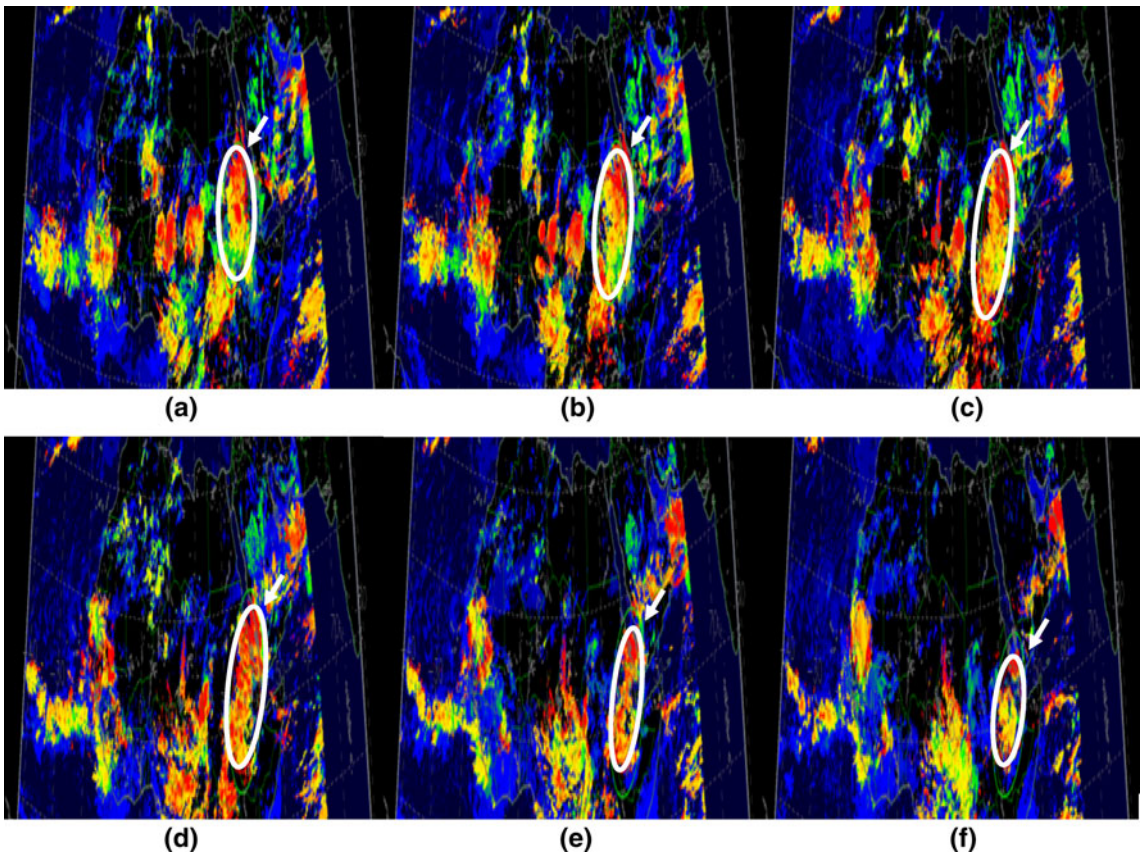

Fig. 11 Six frames produced by the SOAMST algorithm when applied to the Meteosat second generation cloud top height image sequence representing **a** 8/14/00Z, **b** 8/13/21Z, **c** 8/13/18Z, **d** 8/13/15Z, **e** 8/13/12Z, and **f** 8/13/09Z with *white arrow* and *circle* indicating tracked cloud

proposed by Ning et al. (2010). The results generated using these techniques were quite accurate. All of the results after applying the SOAMST algorithm concluded that the origin of pre-TS Debby is located at (10°N, 40°E), and that this location was reached on 8/12/15Z except for results based on the IR and CTH image sequences. The IR image sequence reached this location on 8/12/21Z and the CTH image sequence reached this location on 8/13/09Z. We infer that the IR image sequence reached this location at a different time, since some MCSs are not visible at times when there is still moisture present in the atmosphere that allows the MCS to remain active. This location was reached sooner in the CTH image sequence due to the many low-level clouds that are present in the CTH images. The CTH images contain mostly low-level clouds; therefore, when extracting the second central moment in the SOAMST algorithm, these clouds have a stronger effect on the tracking results than the high- and middle-level clouds. Therefore, the valid time when referring to the origin was 8/12/15Z. When there is a difference in the time at the TC originated but the location is the same, the fusion and clustered images should be used to determine the time since they consider the moisture in the atmosphere and the middle and high-level clouds.

5 Conclusions and future work

An objectively analyzed AEW–MCS movement using satellite observations is essential to understanding the formation and propagation of developing TCs. This research has focused on expanding the current research on determining the origins of TCs that develop from AEWs and associated MCSs using solely satellite observations. The image fusion and pattern recognition techniques that were used will improve the accuracy of numerical simulations of pre-TC AEWs and MCSs and can be applied to other AEWs and MCSs leading to tropical cyclogenesis.

We hypothesized that the Ethiopian Highlands and other mountains may play a role in initiating the AEWs and their associated MCSs along with other environmental factors. These factors were analyzed by applying

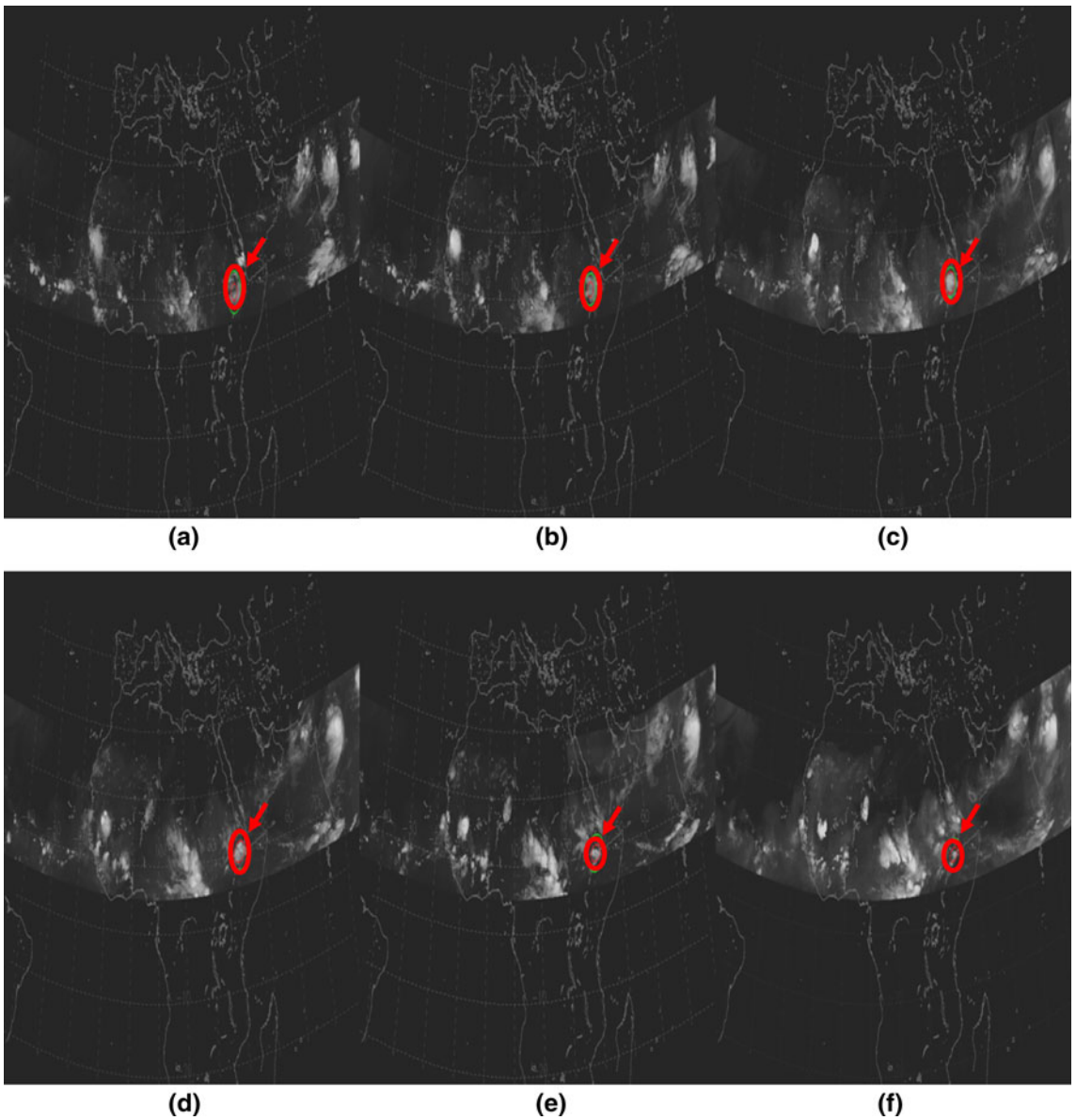

Fig. 12 Six frames produced by the SOAMST algorithm when applied to the fused image sequence representing **a** 8/13/06Z, **b** 8/13/03Z, **c** 8/13/00Z, **d** 8/12/21Z, **e** 8/12/18Z, and **f** 8/12/15Z with *red arrow* and *circle* indicating tracked cloud (color figure online)

image fusion and pattern recognition techniques and the hypothesis was validated. The MCSs of this storm assisted in developing the TS at 21.7°W, 11.6°N on 8/21/18Z. The movement of the pre-TS Debby (2006) AEW–MCS system was analyzed using image fusion, FCM-based clustering, and the SOAMST algorithm. The results confirmed that the pre-TS Debby (2006) MCS formed over the peak of the Ethiopian Highlands. Furthermore, these results verified the latitude of the origin; but, the longitude and date differ when compared to the work by Lin et al. (2012) which was based on the Numerical Weather Prediction models.

In the future, this work could be extended to analyze additional pre-TCs MCSs. A future goal for this research is to interpolate satellite data to get more accurate tracking results and to integrate IDL and Matlab to make implementation easier. With this integration, the forecasters will be able to use the proposed techniques to assist in determining the origins of these TCs. The accuracy of information will help the public prepare for TCs in a timely manner by helping researchers design model domains to include the origin of the TC. The fundamental issue of locating the origin of TCs could be further enhanced through finding the signature of the originating MCS. This

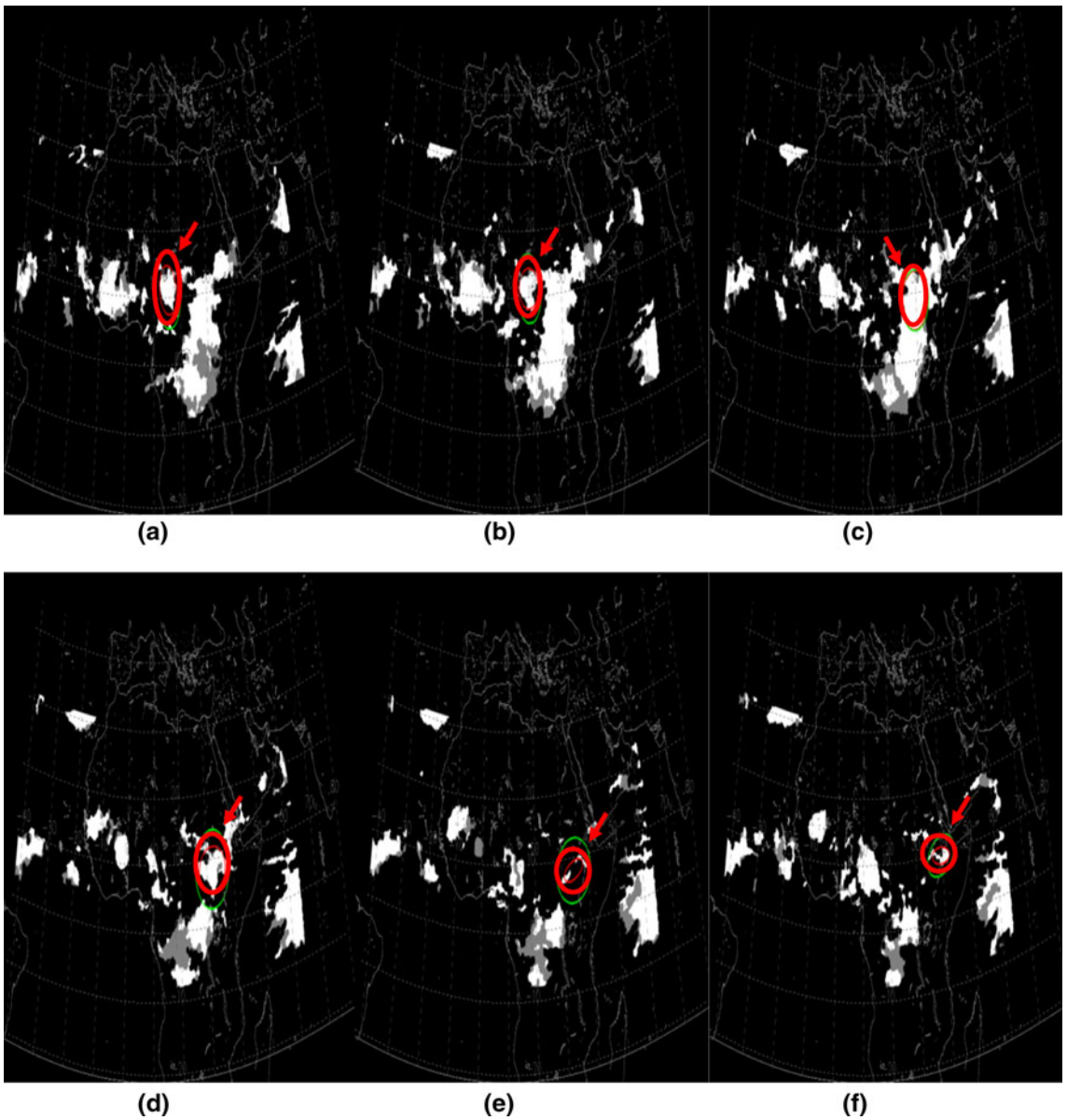

Fig. 13 Six frames produced by the SOAMST algorithm when applied to the clustered cloud top height image sequence representing **a** 8/13/06Z, **b** 8/13/03Z, **c** 8/13/00Z, **d** 8/12/21Z, **e** 8/12/18Z, and **f** 8/12/15Z with *red arrow* and *circle* indicating tracked cloud (color figure online)

work will be extended to address this issue. Also, the model domain which includes the TC's origin will assist the model in making better predictions by allowing a reasonable model initialization scheme.

Acknowledgments The authors are very grateful to the anonymous reviewers for their helpful and insightful recommendations. This research was supported in part by the National Oceanic and Atmospheric Administration Educational Partnership Program under Cooperative Agreement No. NA06OAR4810187 and the Expeditions in Computing program of the National Science Foundation under Award No. CCF 1029731. The contributions to and the assistance of Kenneth R. Knapp of NOAA National Climatic Data Center to this research are greatly appreciated.

References

Agudelo PA, Hoyos CD, Curry JA, Webster PJ (2011) Probabilistic discrimination between large-scale environments of intensifying and decaying African easterly waves. Clim Dyn 36(7): 1379–1401

Albayrak S, Amasyali F (2003) Fuzzy C-means clustering on medical diagnostic systems. In: Proceedings of International XII. Turkish Symposium on Artificial Intelligence and Neural Networks. http://www.ce.yildiz.edu.tr/mygetfile.php?id=269. Accessed 1 April 2011

Burpee RW (1972) The origin and structure of easterly waves in the lower troposphere of North Africa. J Atmos Sci 29:77–90

Berry GJ, Thorncroft C (2005) Case study of an intense African easterly wave. Mon Wea Rev 133(4):752–766

Carlson TN (1969) Synoptic histories of three African disturbances that developed into Atlantic hurricanes. Mon Wea Rev 97(3): 256–276

Grazzini J, Bereziat D, Herlin Z (2001) Analysis of cloudy structures evolution on meteorological satellite acquisitions. In: Proceedings 2001 International Conference on Image Processing, vol 3. pp 760–763

Grist JP (2002) Easterly waves over Africa. Part I: the seasonal cycle and contrasts between wet and dry years. Mon Wea Rev 130(2):197–211

Hall DL, McMullen SAH (2004) Mathematical techniques in multisensor data fusion, 2nd edn. Artech House, Massachussets

Hill CM, Lin Y-L (2003) Initiation of a mesoscale convective complex over the ethiopian highlands preceding the genesis of hurricane Alberto (2000). Geophys Res Lett 30(5):1232

Hodges KI, Thorncroft CD (1997) Distribution and statistics of African mesoscale convective weather systems based on the ISCCP Meteosat imagery. Mon Wea Rev 125(11):2821–2837

ITT Visual Information Solutions. Product Services. http://www.ittvis.com/language/en-US/ProductServices/IDL.aspx. Accessed 1 June 2011

Jirak IL, Cotton WR (2007) Observational analysis of the predictability of mesoscale convective systems. Wea Forecast 22(4):813–838

Lacewell CW, Gebril M, Buaba R, Homaifar A (2010) Optimization of Image fusion using genetic algorithms and discrete wavelet transform. In: Aerospace and Electronics Conference (NAECON), Proceedings of the IEEE 2010 National, pp 116–121

Laing AG, Fritsch JM (1993) Mesoscale convective complexes in Africa. Mon Wea Rev 121(8):2254–2263

Landsea CW (1993) A climatology of intense (or major) Atlantic hurricanes. Mon Wea Rev 121(6):1703–1713

Lin Y-L (2007) Mesoscale dynamics. Cambridge University Press, New York

Lin Y-L, Robertson KE, Hill CM (2005) Origin and propagation of a disturbance associated with an African easterly wave as a precursor of hurricane Alberto 2000. Mon Wea Rev 133(11): 3276–3298

Lin Y-L, Liu L, Tang G, Spinks J, Jones W (2012) Origin of the pre-tropical storm Debby (2006) African easterly wave–mesoscale convective system. Meteor Atmos Phys (in review)

Mandal AK, Pal S, De AK, Mitra S (2005) Novel approach to identify good tracer clouds from a sequence of satellite images. IEEE Trans Geosci Remote Sens 43(4):813–818

MathWorks Incorporated, MATLAB The Language of Technical Computing. http://www.mathworks.com/products/matlab. Accessed 1 June 2011

Mozer JB, Zehnder JA (1996) Lee vorticity production by large-scale tropical mountain ranges. Part II: a mechanism for the production of African waves. J Atmos Sci 53(4):539–549

Mumtaz A, Majid A, Mumtaz A (2008) Genetic algorithms and its application to image fusion. In: 4th International Conference on Emerging Technologies, 2008, ICET 2008, pp 6–10

Ning J, Zhang L, Zhang D, Wu C (2010) Scale and orientation adaptive mean shift tracking. Comput Vis IET 6(1):52–61

Pielke RA, Landsea CW (1998) Normalized hurricane damages in the United States. 1925–95. Wea Forecast 13(3):621–631

Piñeros M, Ritchie EA (2006) Quantifying morphologic features of remotely-sensed data for its use in a tropical cyclogenesis predictor. http://ams.confex.com/ams/pdfpapers/108814.pdf. Accessed 20 May 2011

Piñeros MF, Ritchie EA, Tyo JS (2010) Detecting tropical cyclone genesis from remotely sensed infrared image data. IEEE Geosci Remote Sens Lett 7(4):826–830

Pytharoulis I, Thorncroft C (1995) The low-level structure of African easterly waves. Mon Wea Rev 127(10):2266–2280

Reed RJ, Norquist DC, Recker EE (1977) The structure and properties of African wave disturbances as observed during phase III of GATE. Mon Wea Rev 105(3):317–333

Simpson RH, Frank N, Shideler D, Johnson HM (1968) Atlantic tropical disturbances 1967. Mon Wea Rev 96(4):251–259

Theodoridis S, Koutroumbas K (2003) Pattern recognition, 2nd edn. Academic Press, San Diego

Wehrmann T, Colditz R, Bachman M, Steinnocher K, Dech S (2004) Evaluation of image fusion T. In: Proceedings of the 1st Göttingen GIS and Remote Sensing Days

Zawislak J, Zipser EJ (2010) Observations of seven African easterly waves in the east Atlantic during 2006. J Atmos Sci 67(1):26–43